New Developments in Mathematical Modeling of Groundwater Systems

Prof. Abdelkader LARABI

Regional Water Centre of Maghreb

Mohammed V University in Rabat

E-mail: larabi@emi.ac.ma, www.emi.ac.ma/water

Doha, 28 – 30 April 2024

Overview

- **Introduction:** Aquifers, heterogeneity, Anisotropy, complex structures
- **Part I: Deforming Mixed-Hybrid Finite Element Model for GW Flow (novel):**
  - Improve FEM to deal with Non linear problems in unconfined aquifers
  - MHFE Approach, Validation, Benchmarking and Field applications
  - MHFE for Heat Transfer with application to well doublets in the Paris basin (France)
- **Part II: Vulnerability approaches to SWI in Coastal Aquifers**
  - Galdit Approach: weak points and field Applications (Morocco)
  - New approach for Coastal Aquifer vulnerability to Seawater intrusion (Novel): with advanced practices for modeling variable density processes (applications)
- **Concluding Remarks**

Problem setting & Objectives

Illustration of different approaches for modeling unconfined groundwater flow in subsurface aquifers

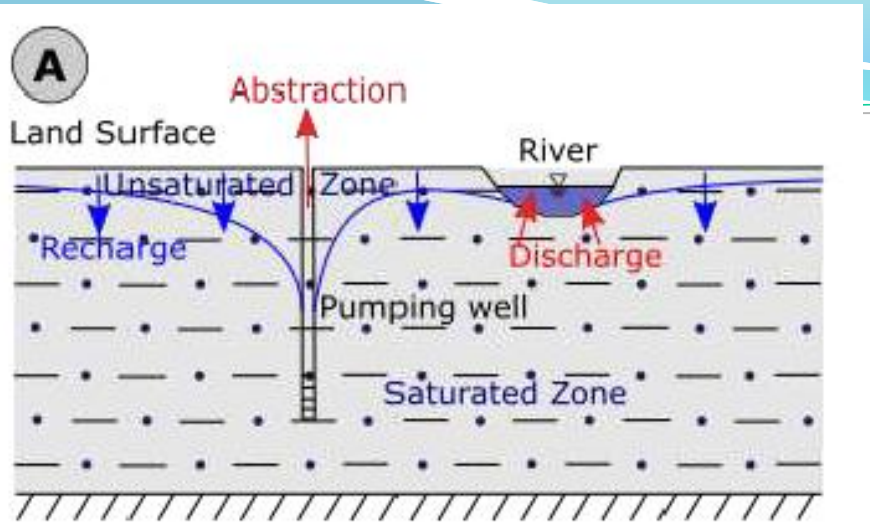

(A) An example of flow processes occurring in an unconfined aquifer such as recharge, abstraction, and aquifer-river interactions.

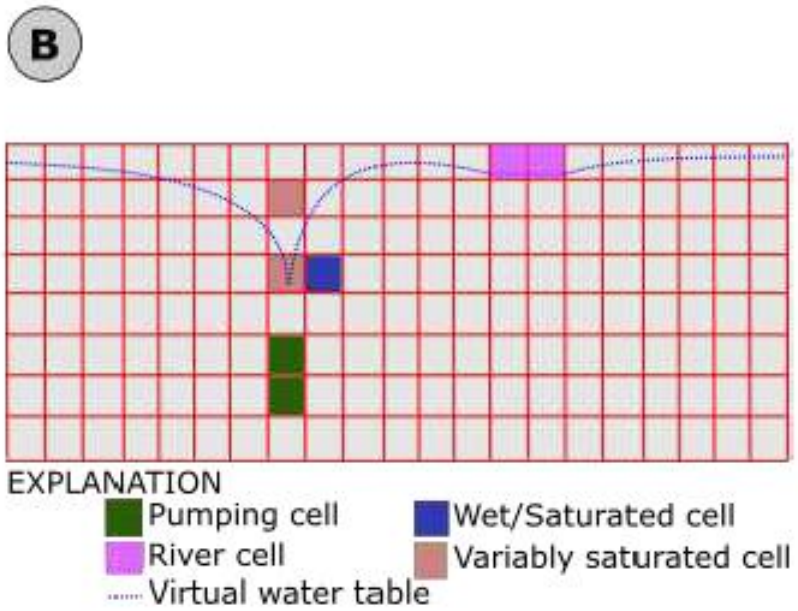

(B) A discrete variably saturated groundwater flow model seeks to determine the saturation state in all cells.

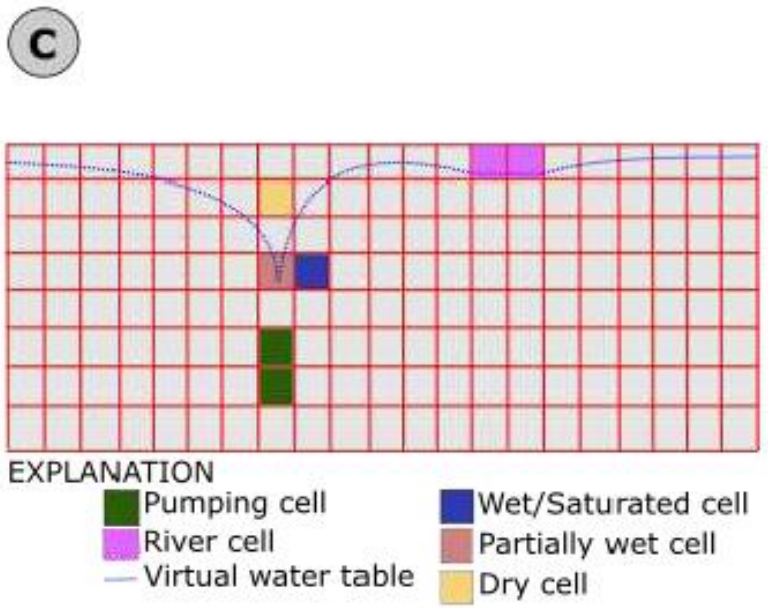

(C) A discrete unconfined flow model neglecting processes in the unsaturated zone using a fixed mesh. The numerical model identifies wet, partially wet, and dry cells.

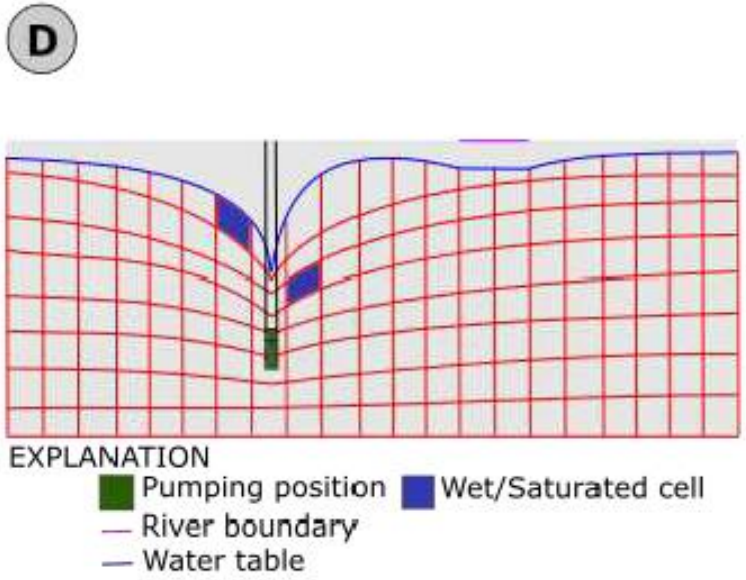

(D) A discrete unconfined flow model neglecting processes in the unsaturated zone using a moving mesh. The numerical model works exclusively with fully saturated cells.

Theory

Governing equation for 3D Groundwater flow in the heterogeneous and anisotropic deforming domain:

$$S_p \frac{\partial h}{\partial t} = \nabla.(\mathbf{K}.\nabla h) + q_s$$

This equation is subject to the initial and boundary conditions of Dirichlet, Neumann, and Cauchy types

- Phreatic Surface Boundary

$$h(x, y, z_{WT}, t) = z_{WT}(x, y, t)$$

$$S_y \frac{\partial h}{\partial t} = (\mathbf{K}.\nabla h + \mathbf{N}).\nabla(h - z)$$

$$S_y \frac{\partial h}{\partial t} = -(K_z + N)\frac{\partial h}{\partial z} + N$$

$$q_z = -N + N\frac{\partial h}{\partial z} + S_y \frac{\partial h}{\partial t}$$

$$q_z = -\left(K_{zx}\frac{\partial h}{\partial x} + K_{zy}\frac{\partial h}{\partial y} + K_{zz}\frac{\partial h}{\partial z}\right)$$

$$q_z = -N + N\frac{\partial h}{\partial z}$$

- Seepage Face

$$h(x, y, z_{WT}, t) = z_{TOP}(x, y)$$

- Recharge

$RE(x, y, t)$ [LT^{-1}],

$RE(x, y, t - t_u(x, y))$.

Discretization of PDEs and Domain aquifer

O **Finite Elements:**

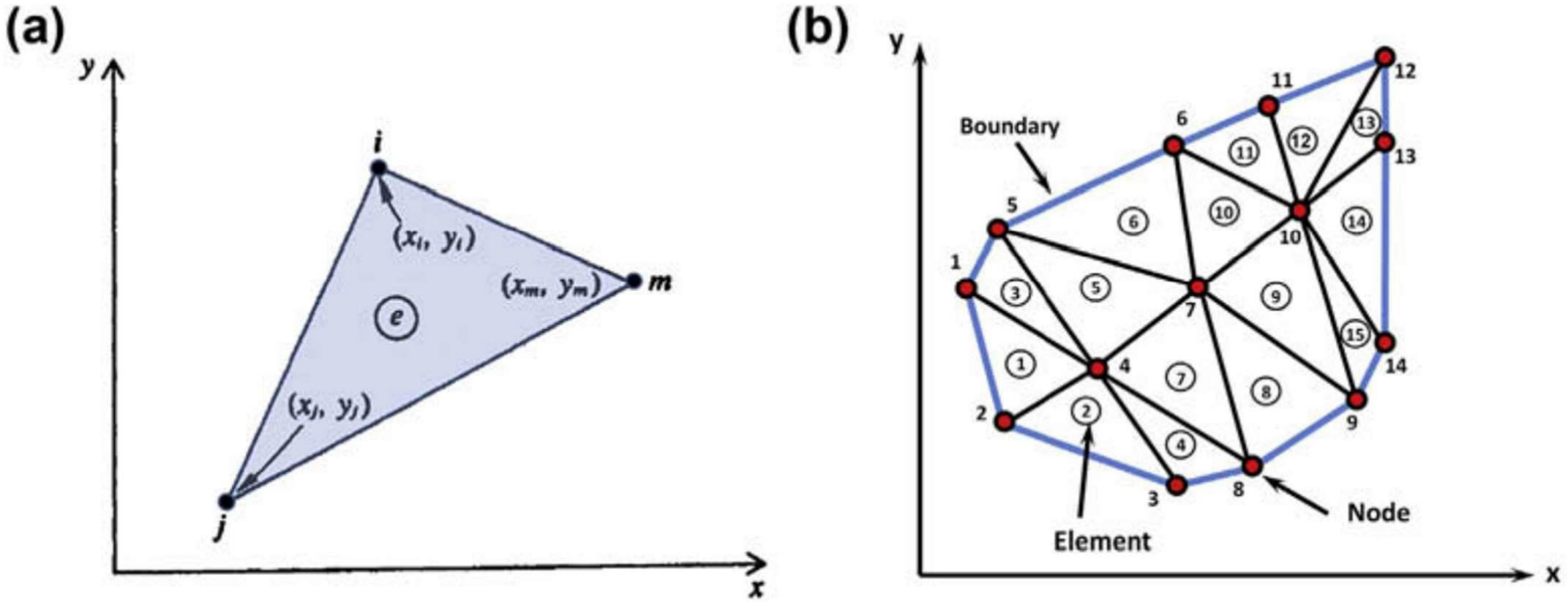

(Anderson et al., 2015)

2D horizontal FE mesh with triangular elements and notation. **(a)** A representative triangular element with nodes i, j, and m, labeled in counterclockwise order, with spatial coordinates (x,y). **(b)** Triangular elements, with element numbers inside circles, are defined by numbered nodes.

NB: **The elements are fitted to the boundary of the same problem domain as dealt by FD.**

Methodology

- *Mixed-Hybrid Finite Element Approximation (MHFE)*

$$q_e = \sum_{j=1}^{6} q_{e,j}\, \boldsymbol{b}_j$$

$$\int_e \nabla . \boldsymbol{b}_j \, de = \int_{f_i} \boldsymbol{b}_j . \mathbf{n}_i \, df_i = \delta_{ij} \quad i,\ j = 1,\ \ldots,\ 6$$

$$\int_e \left(\mathbf{K}_e^{-1} . \boldsymbol{q}_\mathbf{e} \right) . \boldsymbol{b}_i \, de = h_e \int_e \nabla . \boldsymbol{b}_i \, de - \sum_{j=1}^{6} Th_{e,j} \int_{f_j} \boldsymbol{b}_i . \mathbf{n}_j \, df_j \quad i = 1,\ \ldots,\ 6$$

$$\sum_{j=1}^{6} q_{e,j} \int_e \left(\mathbf{K}_e^{-1} . \boldsymbol{b}_j \right) . \boldsymbol{b}_i \, de = h_e - Th_{e,i} \quad i = 1,\ \ldots,\ 6$$

$$A_{ij} = \int_e \left(\mathbf{K}_e^{-1} . \boldsymbol{b}_j \right) . \boldsymbol{b}_i \, de$$

$$q_{e,i} = \alpha_{e,i} h_e - \sum_{j=1}^{6} A_{ij}^{-1}\, Th_j$$

$$\alpha_{e,i} = \sum_{j=1}^{6} A_{ij}^{-1}$$

$$q_{e_1,i} + q_{e_2,i} = 0$$

$$\alpha_{e_1,i} h_{e_1} + \alpha_{e_2,i} h_{e_2} - \sum_{j=1}^{6} \left[\left(A_{ij}^{-1} \right)_{e_1} - \left(A_{ij}^{-1} \right)_{e_2} \right] Th_j = 0$$

$$\alpha_{e,i} h_e - \sum_{j=1}^{6} A_{ij}^{-1} \, Th_j = q_N$$

$$\alpha_{e,i} h_e - \sum_{j=1}^{6} A_{ij}^{-1} \, Th_j - \lambda_i Th_i = -\lambda_i Th_{i,0}$$

$$[G]\{h\} - [H]\{Th\} = \{D\} + \{N\} + \{C\}$$

$$G_{ij} = \begin{cases} \alpha_{e_j,i} & f_i \in \partial e_j \\ 0 & f_i \notin \partial e_j \end{cases} \qquad H_{ij} = \begin{cases} \sum_{f_i,\, f_j \in \partial e} \left(A_{ij}^{-1} \right)_e - \lambda_i & f_i \in \Gamma_C \\ \sum_{f_i,\, f_j \in \partial e} \left(A_{ij}^{-1} \right)_e & f_i \notin \Gamma_C \end{cases}$$

$$D_i = \begin{cases} H_{ij} \, Th_{i,0} & f_i \in \Gamma_D \\ 0 & f_i \notin \Gamma_D \end{cases} \qquad N_i = \begin{cases} q_i & f_i \in \Gamma_N \\ 0 & f_i \notin \Gamma_N \end{cases} \qquad C_i = \begin{cases} \lambda_i Th_{i,0} & f_i \in \Gamma_C \\ 0 & f_i \notin \Gamma_C \end{cases}$$

- Integration of Equation (1), using a first-order fully implicit Euler discretization in time

❖Results

- Pumping in 2D Anisotropic Aquifer

$$s(x,y,t) = \frac{Q_w}{4\pi\sqrt{T_{xx}T_{yy} - T_{xy}^2}} W(u)$$

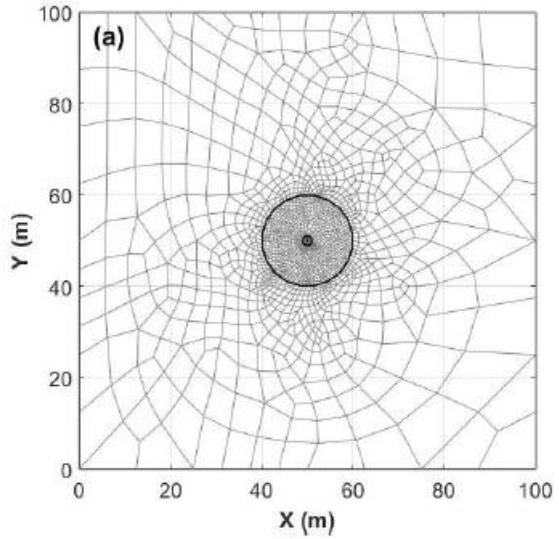

(a) Plan view of the unstructured mesh used for simulating the hydraulic head drawdown in an anisotropic aquifer.

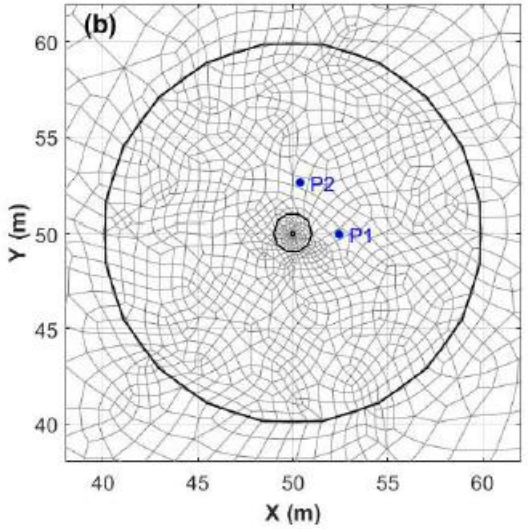

(b) Enlarged view around the first level of mesh refinement within a 10 m radius from the domain center. The two piezometers are shown.

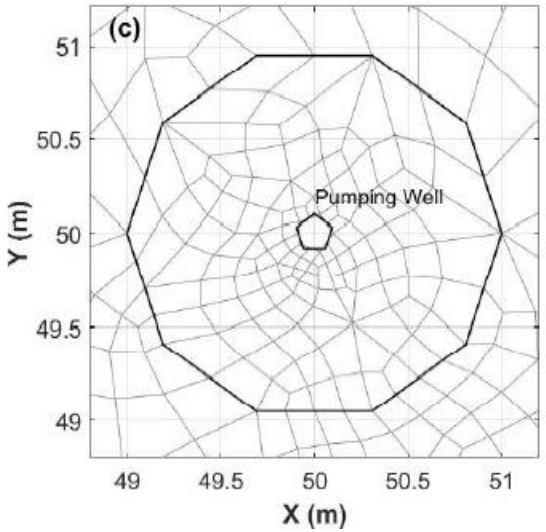

(c) Enlarged view around the second level of mesh refinement within a 1 m radius from the domain center. The well is approximated with a regular pentagon and has a radius of 0.1 m.

The hydraulic head drawdown in an anisotropic aquifer: comparison of the Papadopulos analytical solution with results of the MHFEM model at piezometers P1 and P2

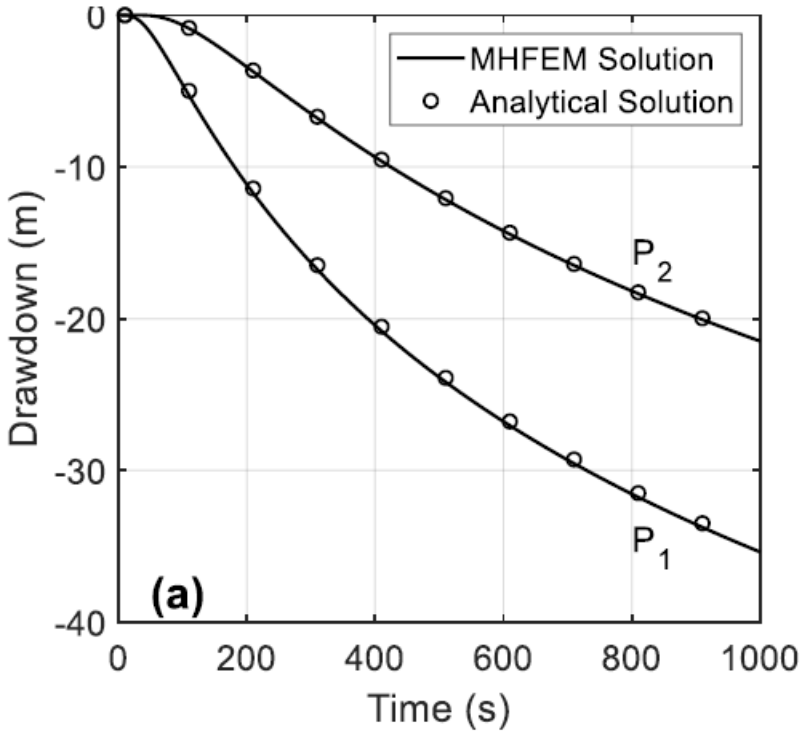

with (a) a diagonal transmissivity tensor,

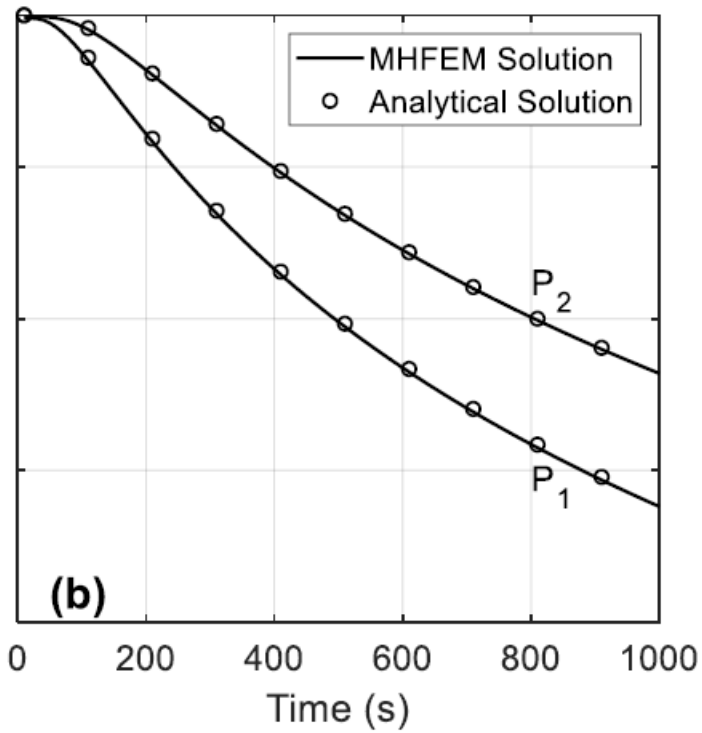

and (b) a full symmetric transmissivity tensor.

- **2D Free Surface in a Pumped Phreatic Aquifer**

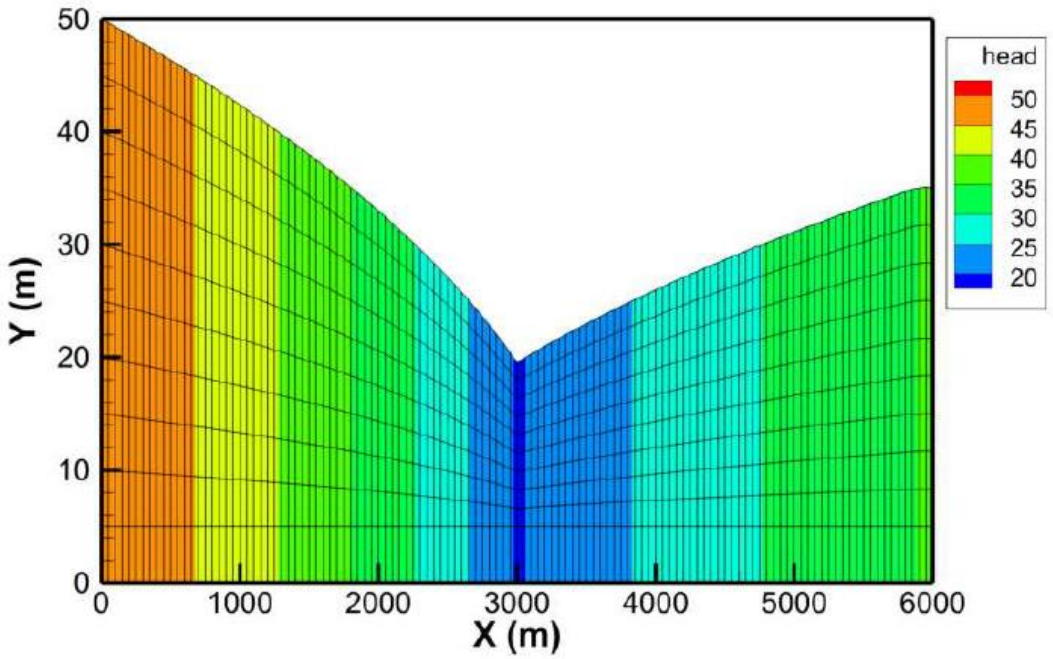

Simulated steady-state water table position and groundwater heads using the adaptive mesh MHFEM technique for the fourth test problem. All horizontal lines of the two-dimensional mesh were allowed to move during the iterative procedure (vertical aspect ratio = 80).

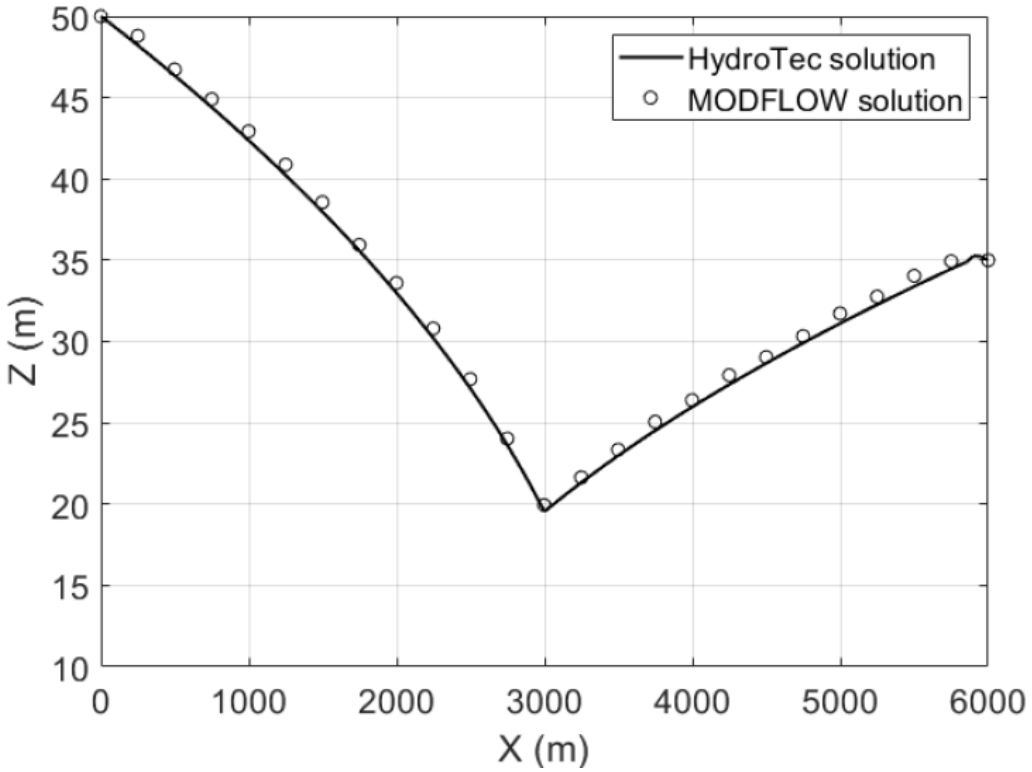

Comparison between the water table simulated with the adaptive MHFEM approximation and the post-processed FDM approximation. There is a good match for the well drawdown. The observed discrepancies far from the well are mainly attributed to post-processing interpolation errors.

- **3D Free Surface in a Pumped Phreatic Aquifer**

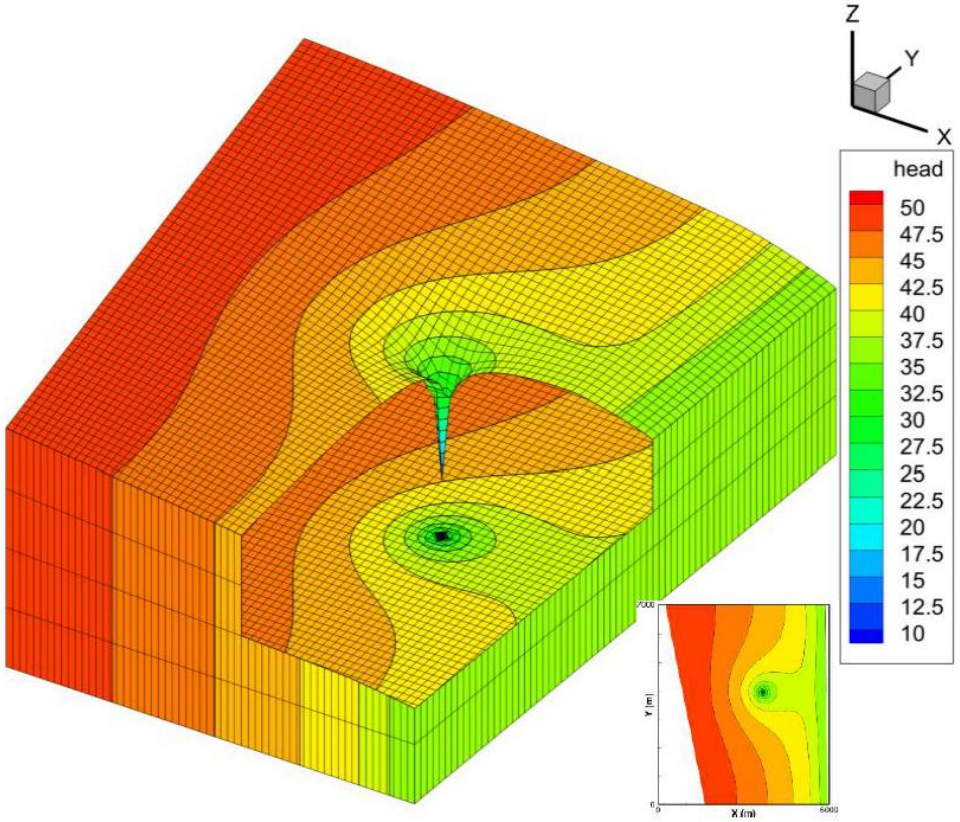

Simulated steady-state water table position and groundwater heads using the adaptive mesh MHFEM technique for the three-dimensional problem. The cutaway view shows the pumping well's depression cone and the head contours at the aquifer base (vertical aspect ratio = 50).

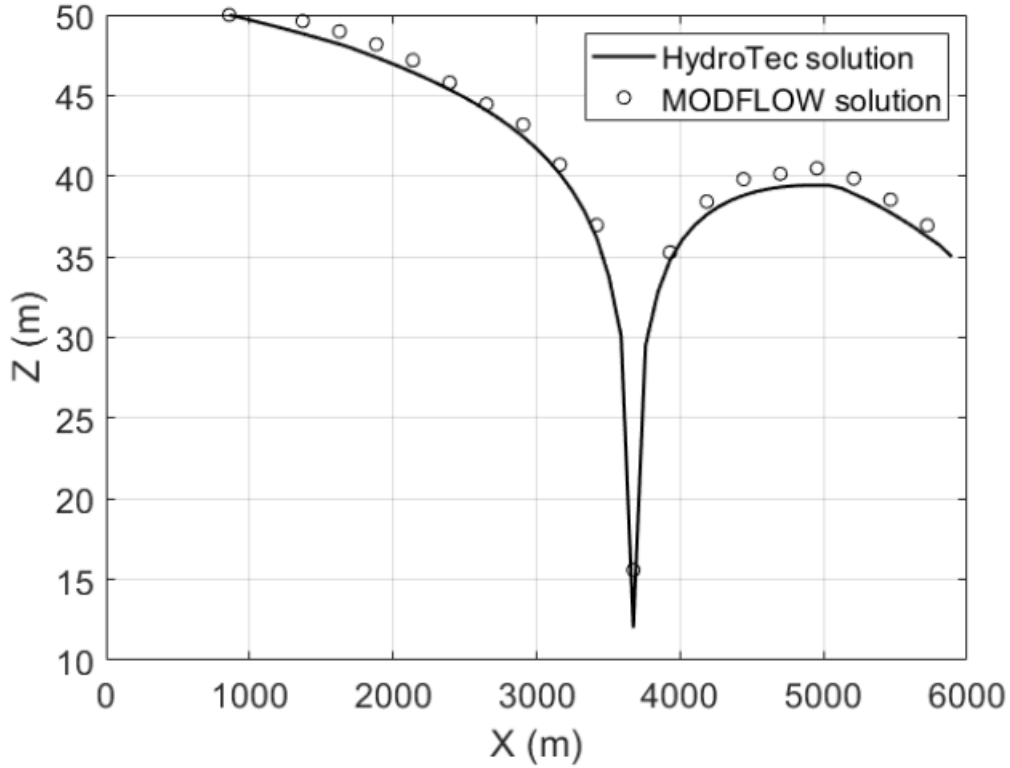

Comparison between the water table profile (parallel to X-axis and crossing the well position) simulated with the adaptive MHFEM approximation and the post-processed FDM approximation for the three-dimensional problem. The maximum difference occurs at the well due to the coarse vertical discretization of the FDM fixed mesh.

- **Heat Transfer with application to well doublets in the Paris basin (France)**
- Study Area: The Meaux doublets in the Dogger reservoir (Paris Basin, France)

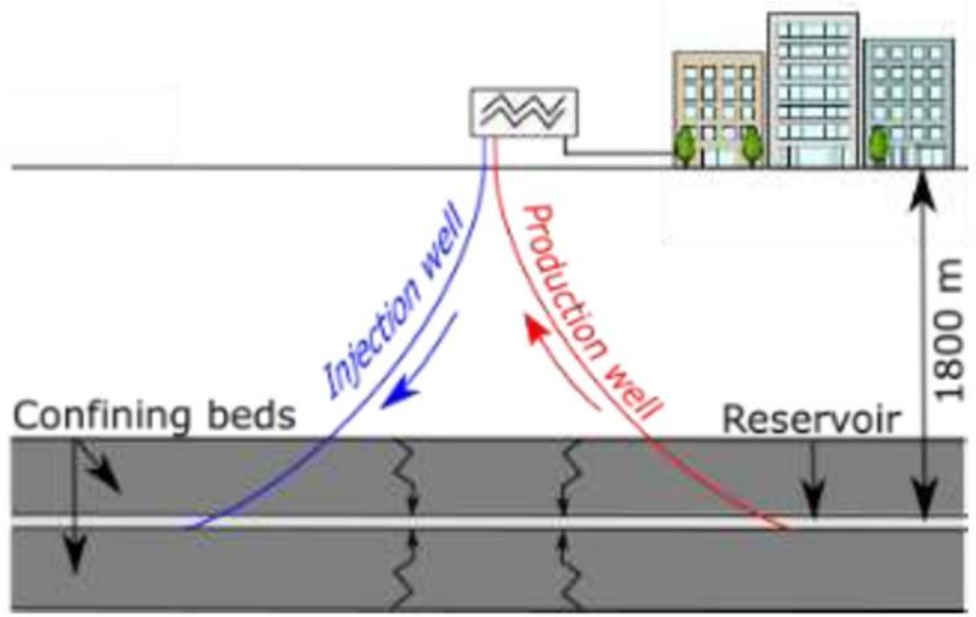

Schematic cross-sectional view of a well-doublet, which utilizes deviated wells for heat extraction and cooled brine reinjection into the Dogger reservoir sandwiched between two confining beds.

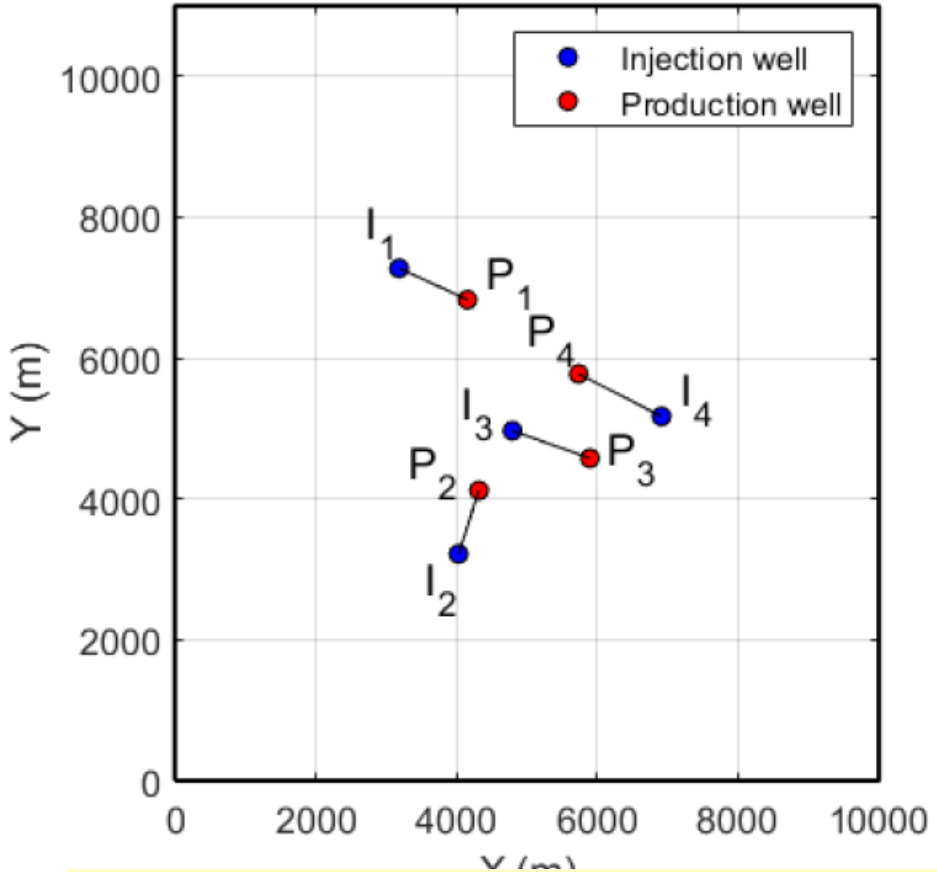

Location of the injection and pumping wells in the study area covering 10 km x 11 km, where they intersect the 1800 m deep Dogger formation.

- **Governing equations**

Groundwater flow equation

$$\rho S_p \frac{\partial h}{\partial t} = \rho \nabla . \left(\mathbf{K} . \nabla h + \delta_\rho \mathbf{K} . \nabla \mathrm{z} \right) + \rho_s q_s$$

governing equation for the distribution of temperature, T, in the aquifer, taking into account the conservation of energy due to convection, conduction, and mechanical dispersion of heat.

$$\rho c \frac{\partial T}{\partial t} + \rho_w c_w \nabla . (\mathrm{q} T) - \nabla . (\lambda . \nabla T) = \rho_w c_w (q_s^+ T_s - q_s^- T)$$

Design of the horizontal unstructured twodimensional mesh utilized in the Meaux doublets, exploiting the Dogger geothermal reservoir. The figure consists of three parts:

Doublet number	Distance between wells	Cosine angle
1	1069.4 m	-24.6°
2	945.6 m	+72.1°
3	1170 m	-19.5°
4	1322.5 m	-27.1°

Geometrical characteristics of the well-doublets in the XY plane.

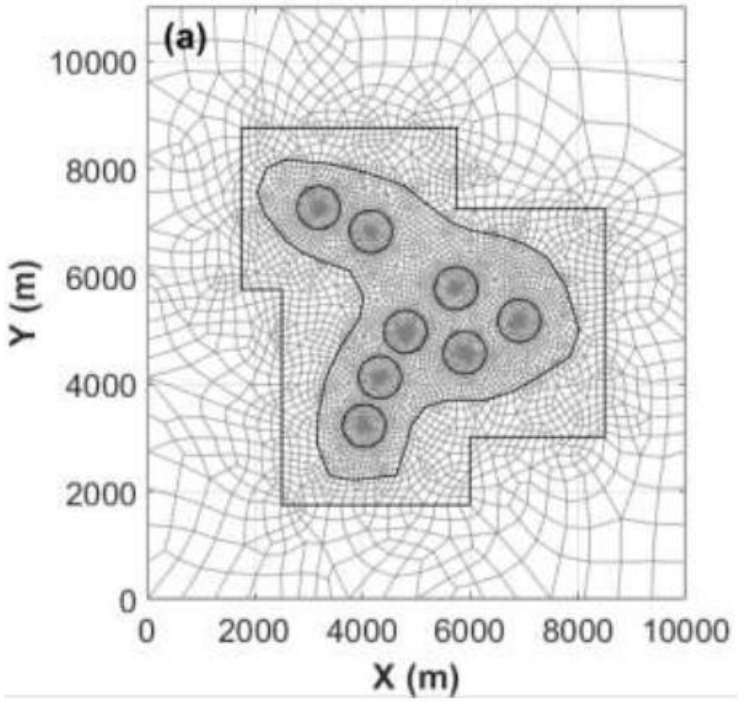

(a) an overall view of the automatically generated mesh with four levels of mesh refinement;

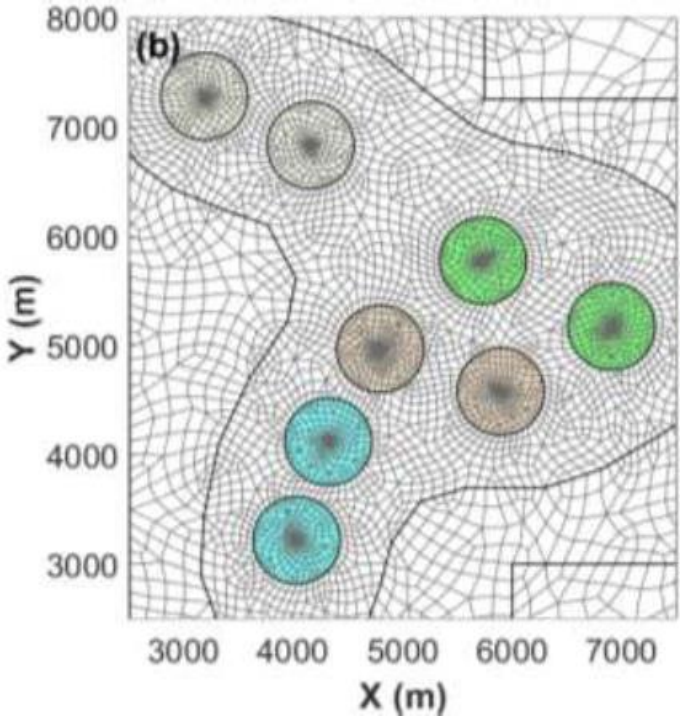

(b) a zoomed-in view around the four well doublets; and

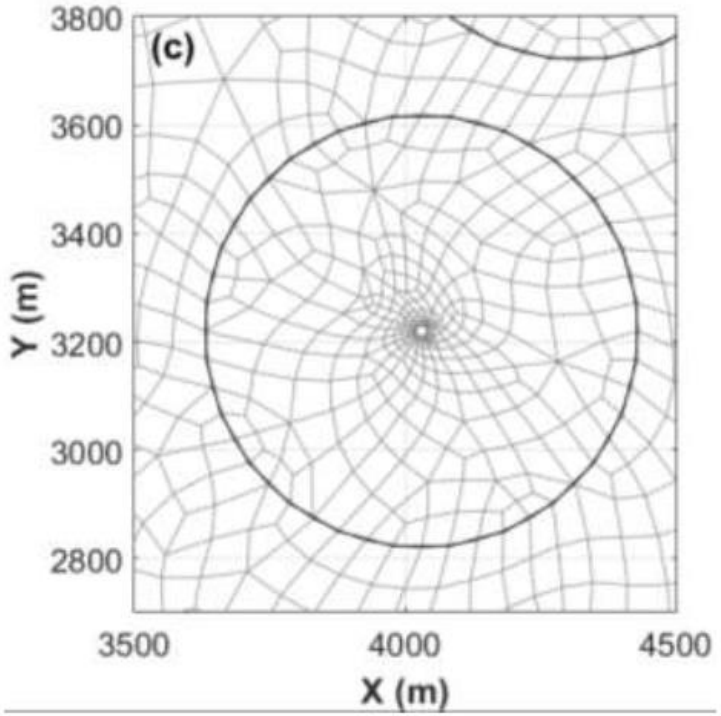

(c) an enlarged view around the injection well I2, displaying the gradual decrease of mesh size starting from the vicinity of the well. The maximal allowed cell sizes for the four mesh refinement levels are 100 m, 150 m, 250 m, and 1500 m, respectively.

Results

Comparison of the simulated cold-water bubbles around the injection wells using the threedimensional coupled hydrothermal model.

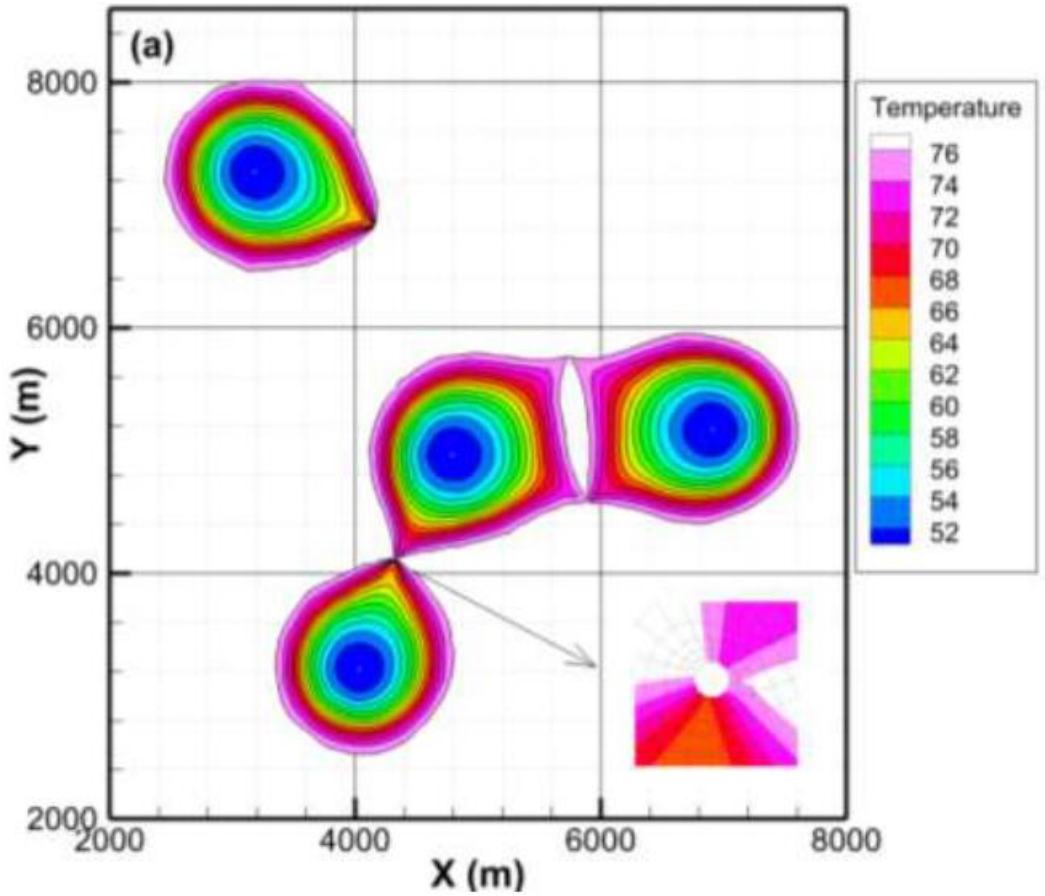

Panel (a) shows the spatial temperature distribution in the reservoir after 30 years of injection obtained using the MHFEM approximation,

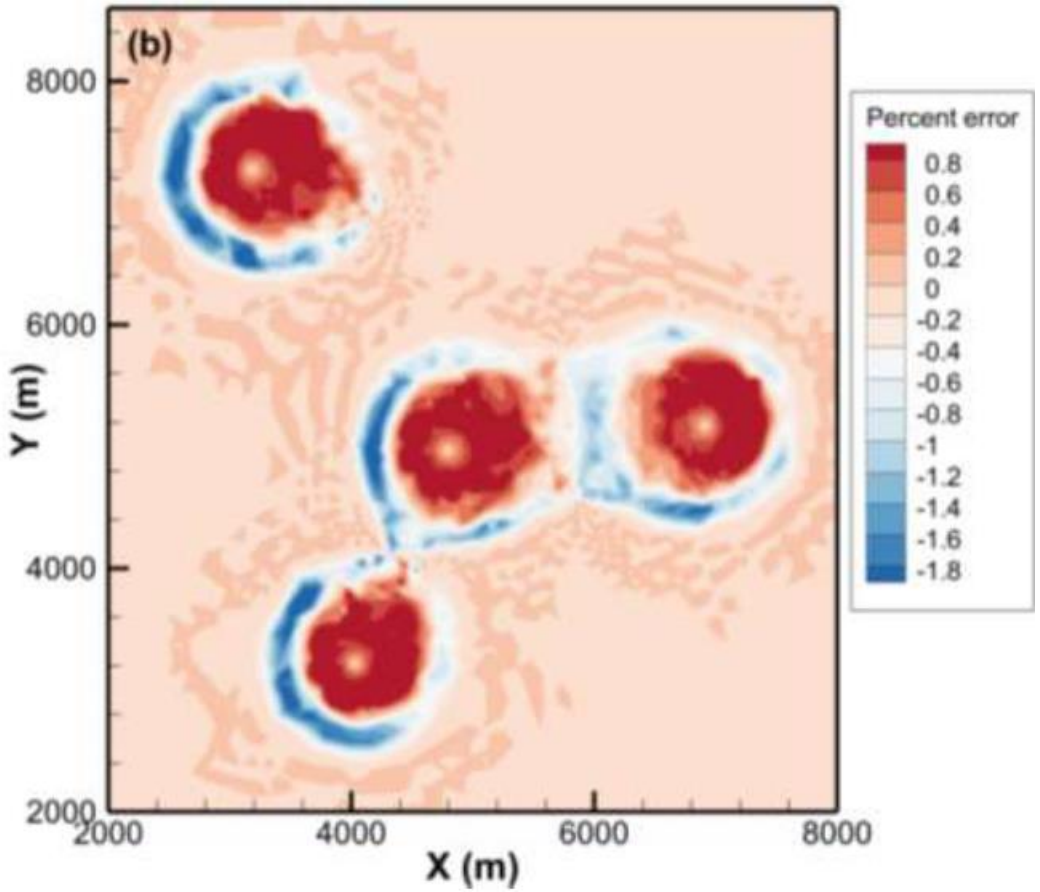

while panel (b) displays the percent error between the MHFEM and the conforming FEM approximations as implemented in HydroTec© and Comsol Multiphysics© software packages, respectively.

Results

- The relationship between the doublet lifetime (LT) and the thermal breakthrough (BT) for the four production wells (a) P1, (b) P2, (c) P3, and (d) P4 in the study area is almost linear.

- Each data point represents a single numerical simulation with a set of uncertain parameters. The results suggest that the horizontal permeability anisotropy and the production flow rate are the most influential factors, followed by the thermal conductivity of the confining beds, while the longitudinal thermal dispersivity and the total productive thickness of the reservoir have a minor impact on the performance metrics.

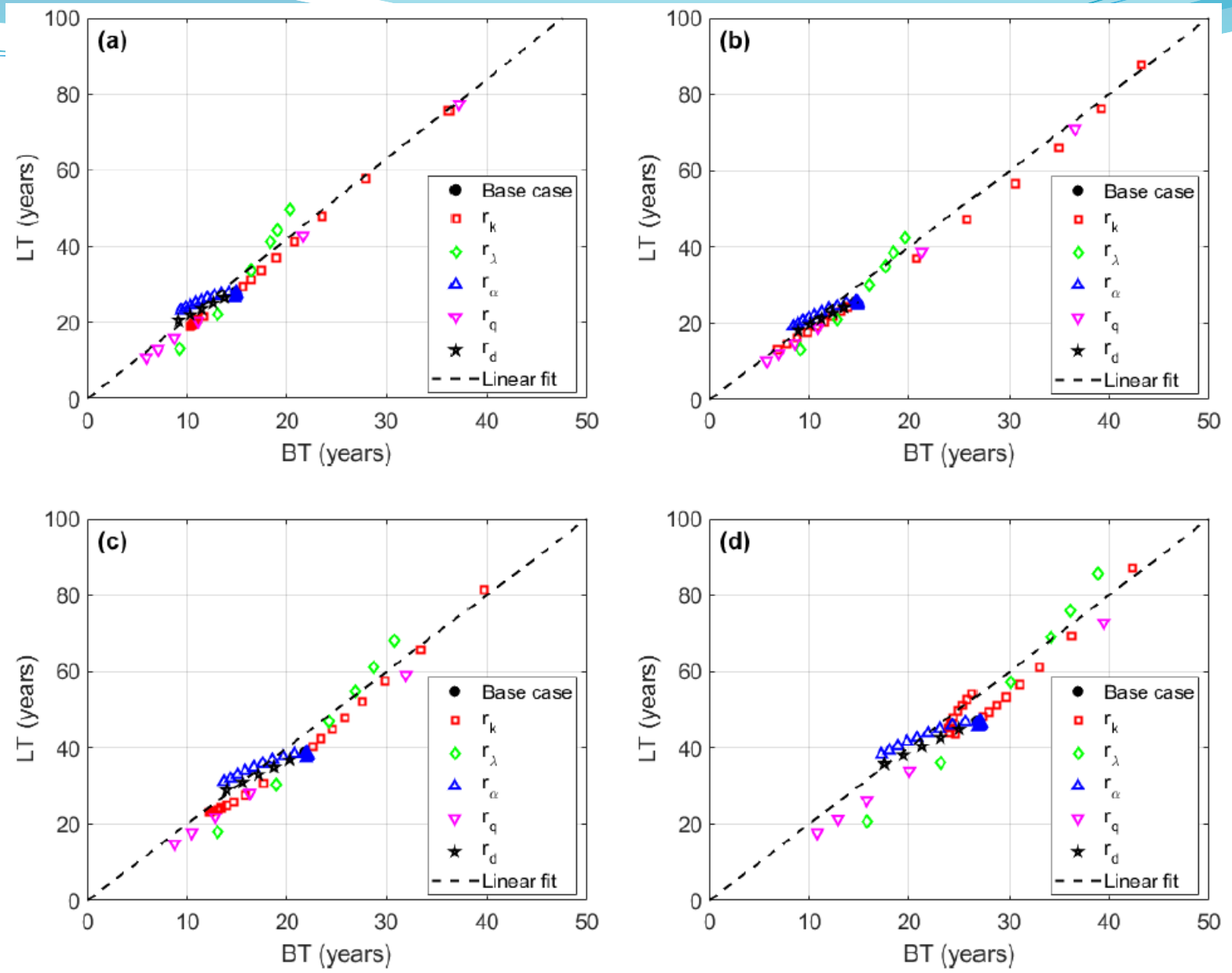

GALDIT METHOD FOR THE VUNERABILITY ASSESSMENT IN THE RMEL COASTAL AQUIFER, MOROCCO

Before: Indexing for aquifer Pollution (DRASTIC, GOD, SINTACS, EPIK…)

Stacking of GALDIT Layers to Produce a Vulnerability Map for SWI

(CHACHADI and LOBO-FERREIRA, 2005)

- **G** → **G**roundwater occurrence (Aquifer Type)
- **A** → **A**quifer hydraulic conductivity
- **L** → Groundwater **L**evel above the sea
- **D** → **D**istance from the shore
- **I** → **I**mpact of existing status of seawater intrusion in the area
- **T** → **T**hickness of the aquifer

Paramètres	Weight	Ranking			
		Very Low	Low	Middle	**High**
		2.5	5	7.5	10
G : Groundwater occurrence – aquifer type	1	Bounded aquifer	Leaky confined	unconfined	confined
A : aquifer hydraulic conductivity (m/day)	3	< 5	5 - 10	10-40	> 40
L : GW level depth/ sea water level (m)	4	< 1	1 – 1.5	1.5 - 2	> 2
D : Distance to the coast (m)	2	< 500	500-750	750-1000	> 1000
I : Impact of sea water intrusion (ppm)	1	< 1	1 – 1.5	1.5 - 2	> 2
T : Thickness of the aquifer (m)	**2**	**< 5**	**5 – 7.5**	**7.5-10**	> 10

$$\text{GALDIT-Index} = \frac{\sum_{i=1}^{6} W_i R_i}{\sum_{i=1}^{6} W_i}$$

Vulnerability classes	GALDIT index
High vulnerability	> 7.5
Moderate vulnerability	5 – 7.5
Low vulnerability	< 5

APPLICATION OF GALDIT METHOD IN RMEL COASTAL AQUIFER, MOROCCO

Stacking of GALDIT Layers (Grid cells = 250 m \ year 2013/2014)

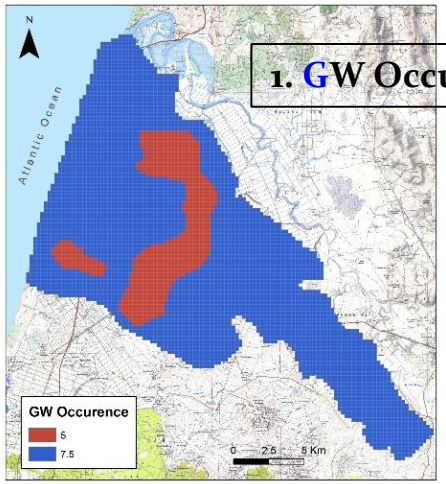

1. GW Occurence

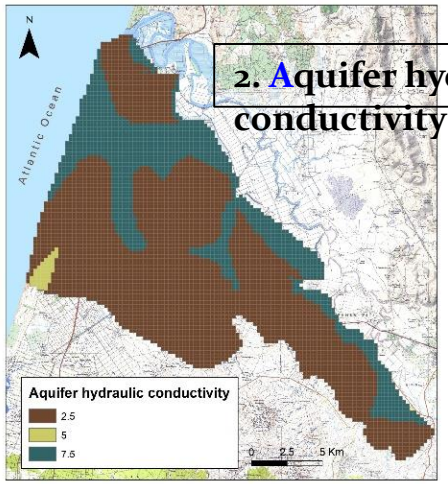

2. Aquifer hydraulic conductivity

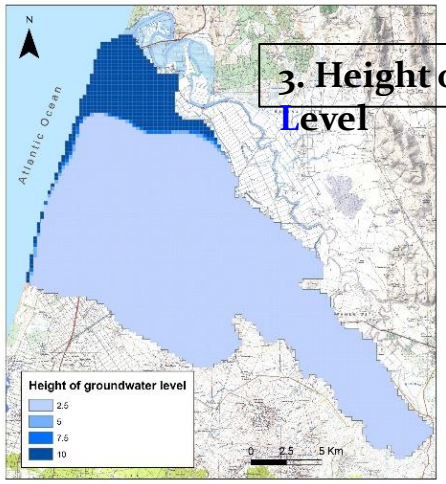

3. Height of GW Level

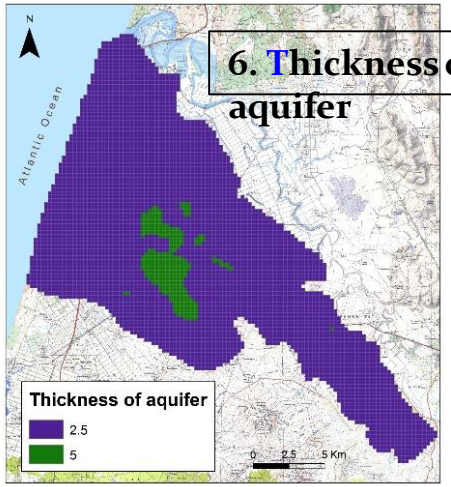

6. Thickness of aquifer

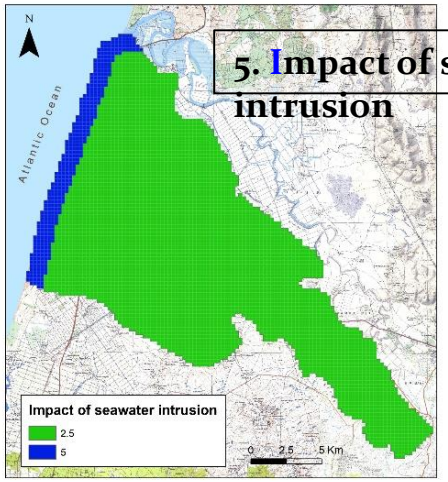

5. Impact of seawater intrusion

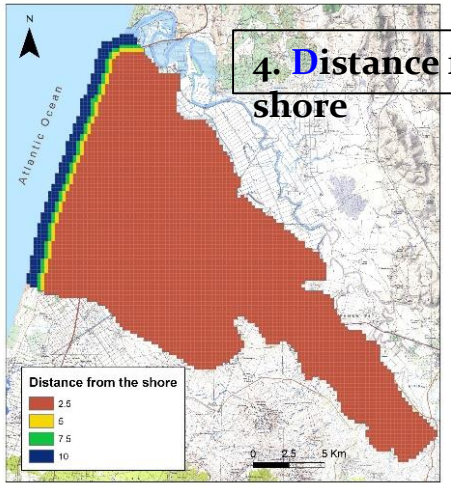

4. Distance from the shore

APPLICATION OF GALDIT METHOD IN RMEL COASTAL AQUIFER, MOROCCO

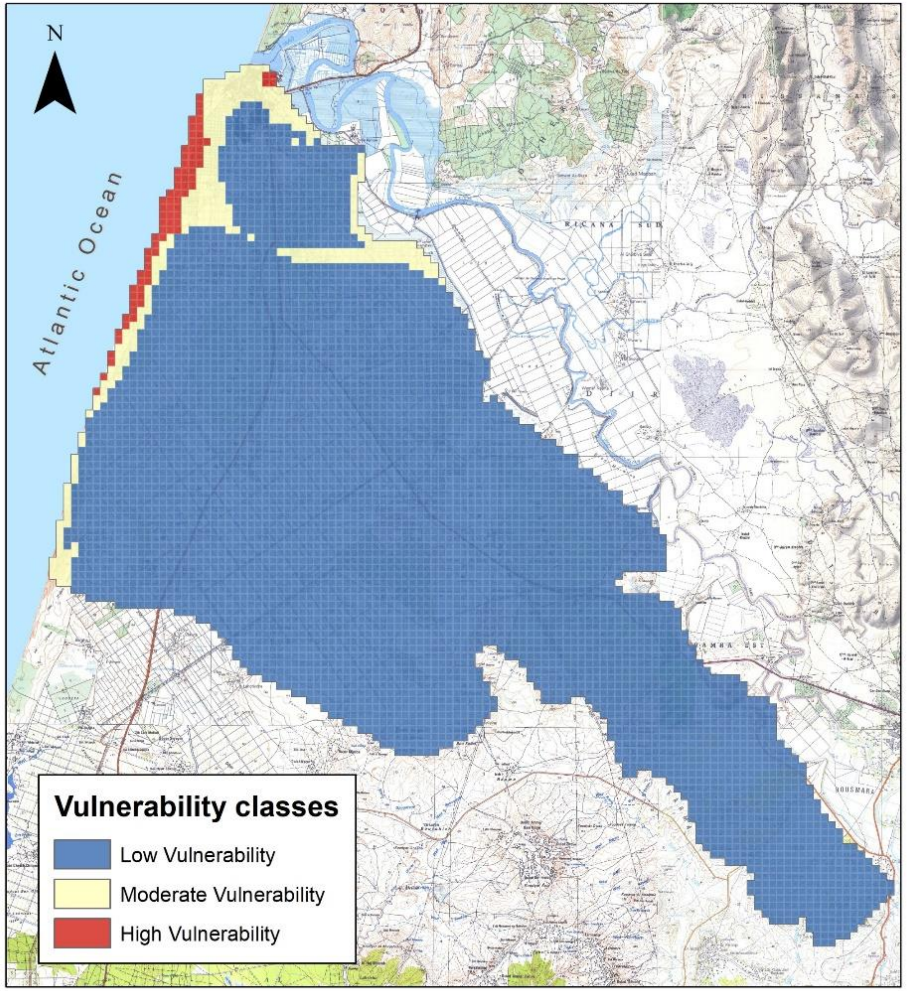

GALDIT specific vulnerability map of GW

GALDIT-Index = $\frac{\sum_{i=1}^{6} W_i R_i}{\sum_{i=1}^{6} W_i}$

The results reveal that the fringe littoral areas of the aquifer are the most affected by seawater intrusion with a high risk in the northwestern part of the study area.

This part is subject to a well fields pumping groundwater for Drinking supply.

APPLICATION OF GALDIT METHOD IN RMEL COASTAL AQUIFER, MOROCCO

Comparison GW modeling and GALDIT method

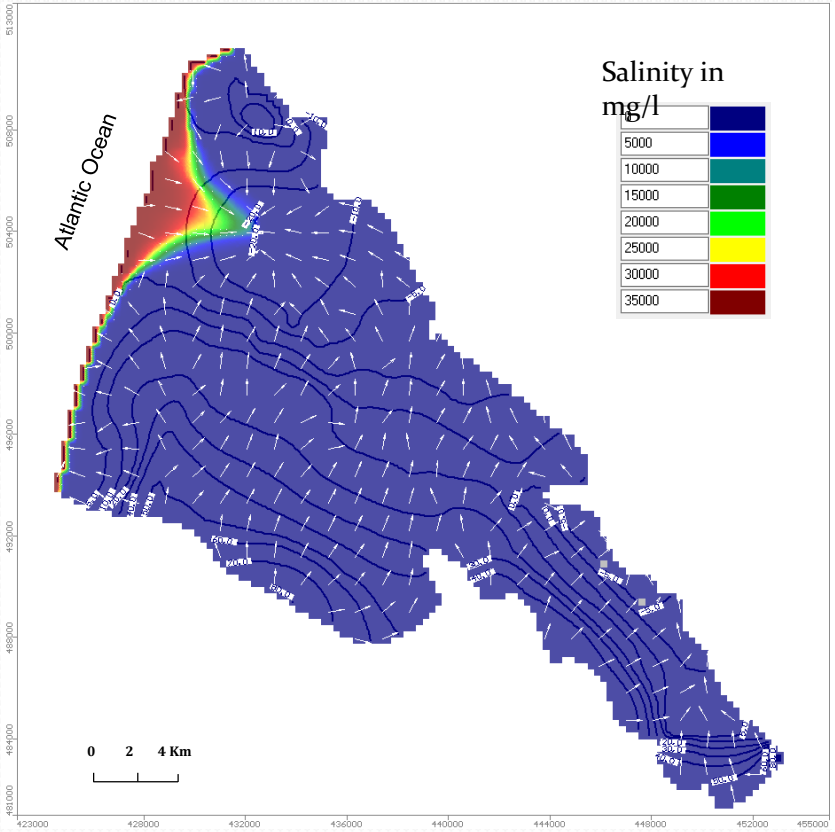

Seawater intrusion modeling (Larabi et al., 2019)

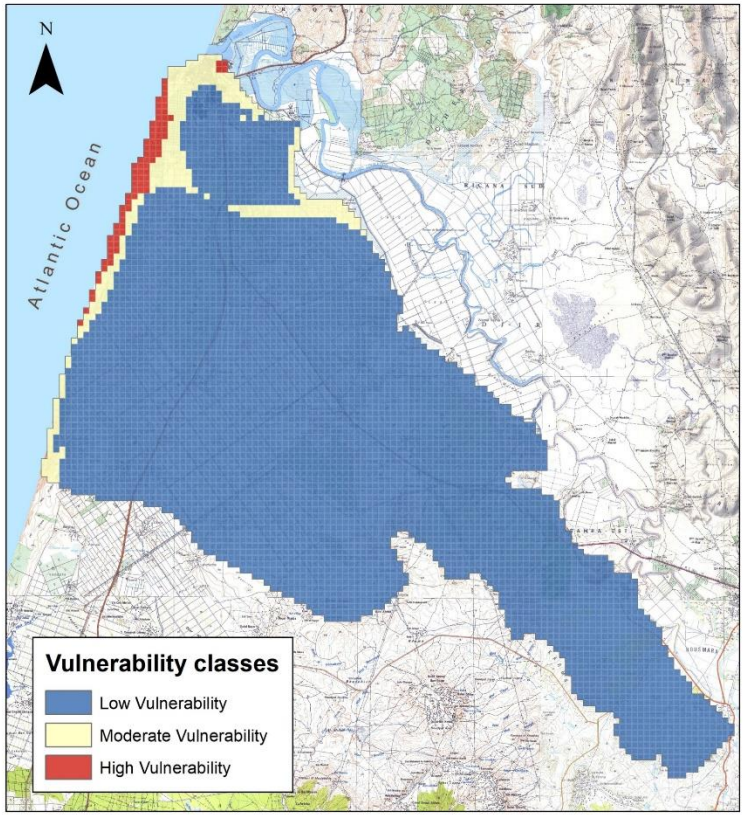

GALDIT method (El Hamidi & Larabi, 2021)

New approach for Coastal Aquifer vulnerability

A recent critical review of many data-driven indexing methods, but not restricted to GALDIT, concluded their limited ability to predict the salinity patterns associated with SWI dynamics exhibiting a weak correlation with field measurements.

STRONG POINTS

- **New approach based on coastal aquifers modeling for quantitative mapping of seawater intrusion vulnerability.**
- **Use steady-state concentrations and mean age of saltwater as a weighting term.**
- **The concept of the zero vulnerability line/interface is introduced for the management of water resources in coastal aquifers.**
- **The advantages of the approach are highlighted using the Henry problem and a field site aquifer**
- **Implications for coastal aquifer management and risk assessments.**

VULNERABILITY OF COASTAL AQUIFER

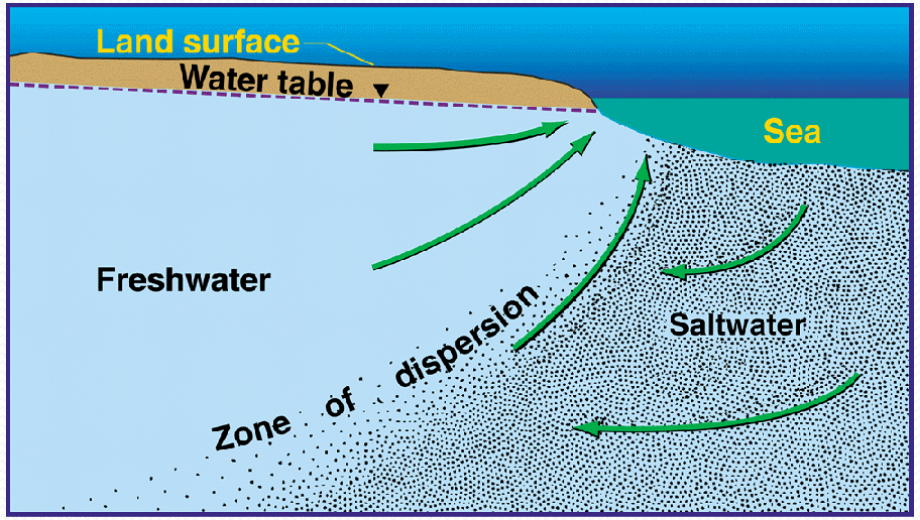

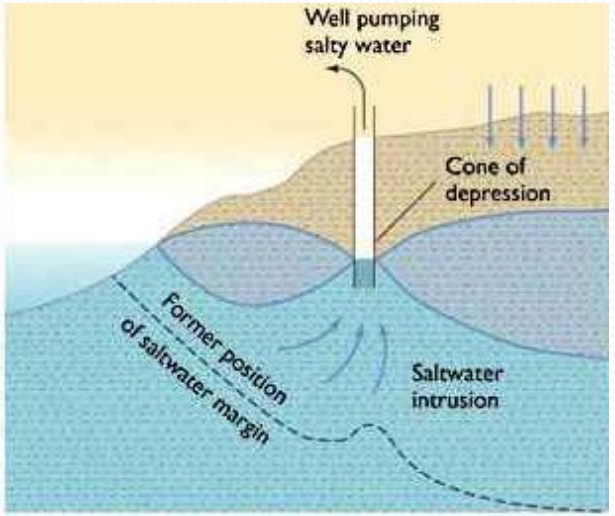

- Steady state process:
  - Density stratification
  - Dispersion zone
  - Submarine discharge zone (s)
  - Salt water recirculation

- Resource exploitation:
  - Cone of depression
  - Upconing

- Why assess vulnerability to seawater intrusion ?
  - Prevention tool against seawater intrusion
  - Prioritize short-term remedial actions

LIMITATION OF INDEXATION TECHNIQUES (i.e. GALDIT)

- Results validation : no consensus for the selection of correlation variables.
- Impossibility of quantifying the water balance, including submarine discharges.
- Errors induced by data interpolation.
- Vulnerability maps are primarily 2D and not representative of the density stratification process.
- Assumptions behind GALDIT are not universal: example of heterogeneous and karst aquifers.

- **Need for a new method based on physical approaches and efficient numerical models (simplified but not simplistic).**

THE NEW METHOD

- Uses a stationary model of flow and mass transport with variable density.
- The distribution of salinity in steady-state cannot be used directly for the vulnerability assessment.
- The age of the salt water is used as a weighting factor for the salinity field.
- Construction of a standardized NSAVI index calculated at each cell of the numerical model.
- Deduction of the line / area of zero vulnerability level.
- Correspondence of the latter with 50% isochlor.
- The method is independent of the spatial discretization (FE, FD, FV) and may be substituted for the modeling tools available in the community.

THE NEW METHOD

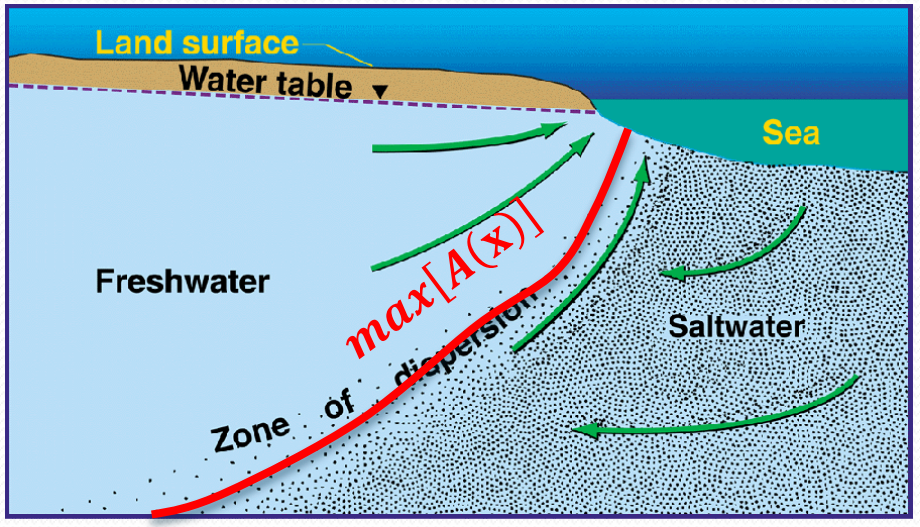

Mass conservation of fluid:

$$\nabla \cdot (\rho \mathbf{q}) = 0$$

Mass conservation of salinity:

$$\nabla \cdot (\mathbf{q}C) - \phi \nabla \cdot (\mathbf{D} \cdot \nabla C) = 0$$

Generalized Darcy's law:

$$\mathbf{q} = -\mathbf{K} \cdot (\nabla H + \rho_r \nabla z)$$

Density-concentration relationship:

$$\rho = \rho_f + \beta(C - C_f)$$

<u>Average</u> age of groundwater:

$$\nabla \cdot (\vec{v}\, A) - \nabla \cdot (\mathbf{D} \cdot \nabla A) = 1$$

Boundary conditions:

$$A = 0 \text{ sur } \Gamma_{in}$$

$$\text{NSAVI}(\mathbf{x}) = \left[1 - \frac{A(\mathbf{x})}{\max[A(\mathbf{x})]}\right] \frac{C(\mathbf{x})}{C_s}$$

Restricting the age of water to the age of salt water

VERIFICATION AND ILLUSTRATION OF CONCEPTS (1)

Henry problem (1964)

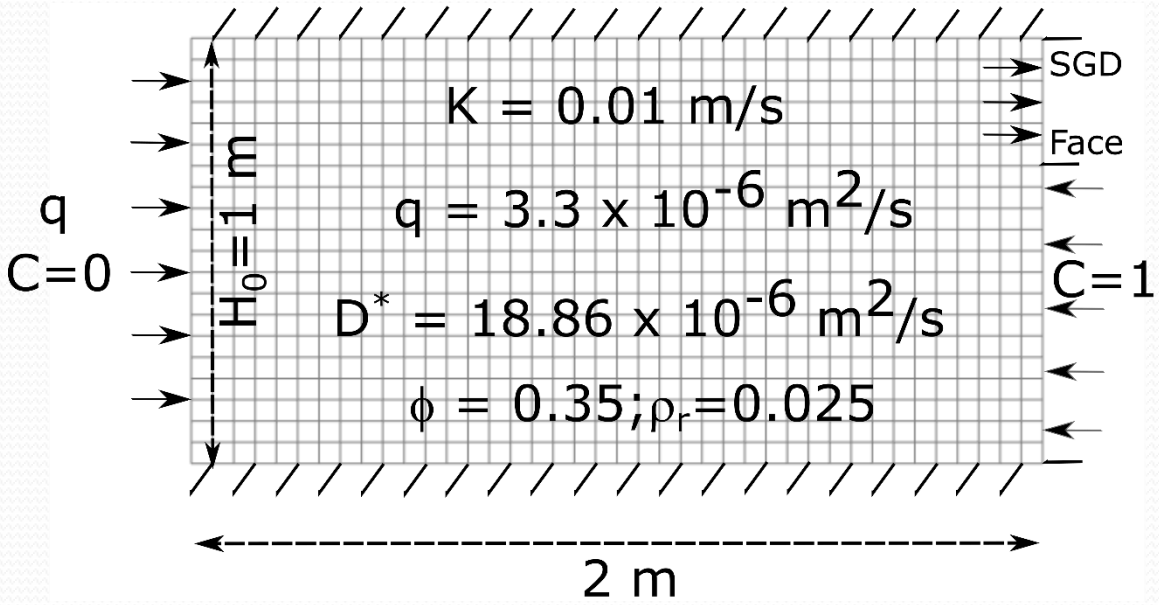

- Academic problem initially proposed to verify numerical models.
- Resumed here to illustrate the NSAVI and ZVL concepts.
- How does ZVL compare to 50% isochlor?

VERIFICATION AND ILLUSTRATION OF CONCEPTS (2)

Henry problem (Homogeneous case # 1)

- Results for Henry's Standard Problem (1964)
- GALDIT predicts the same vulnerability distribution according to z !!!!!!

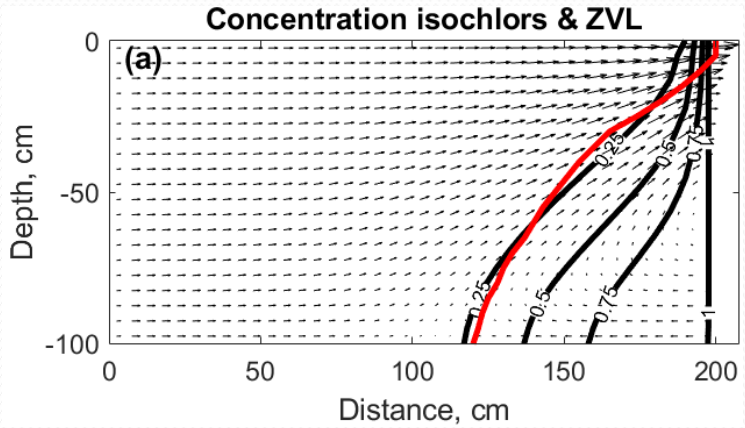

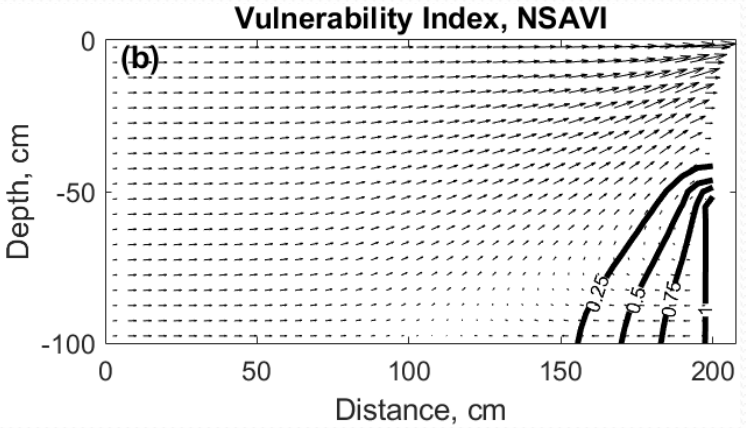

VERIFICATION AND ILLUSTRATION OF CONCEPTS (3)

Henry problem (Homogeneous case # 2)

- Results for Henry's problem with pumping 100 m from the coast
- Flow rate $Q_p = 4 \times 10^{-5}$ m^3/s

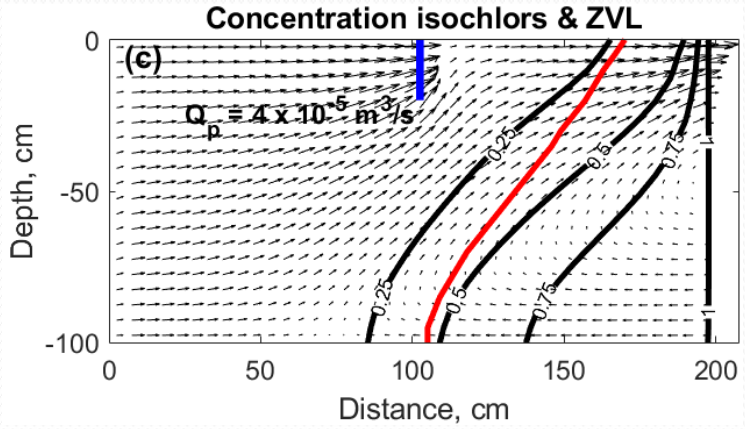

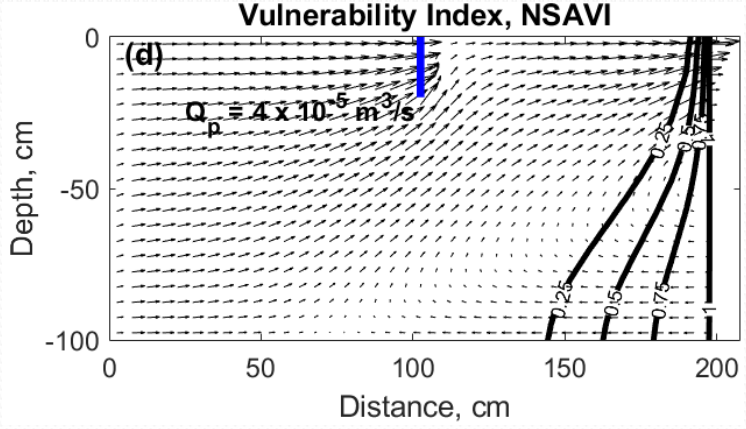

VERIFICATION AND ILLUSTRATION OF CONCEPTS (5)

Henry problem (Heterogeneous case # 1)

- Results for Heterogeneous Henry's Problem: Younes & Fahs (2015)
- Exponential decrease with depth : $k_1 = k_b \exp[+\delta(1-z)]$

δ=3

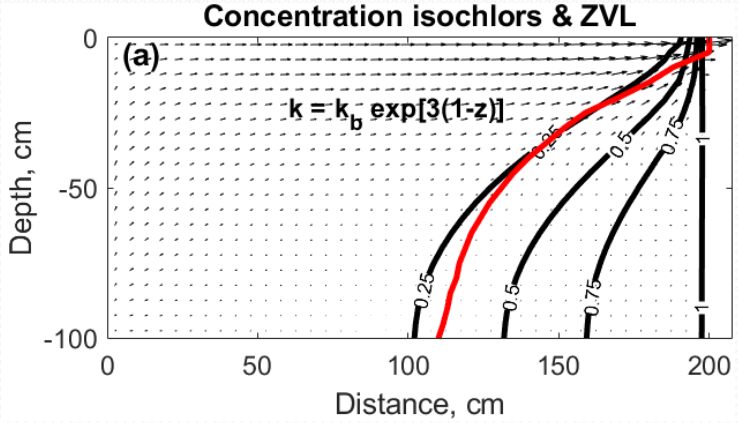

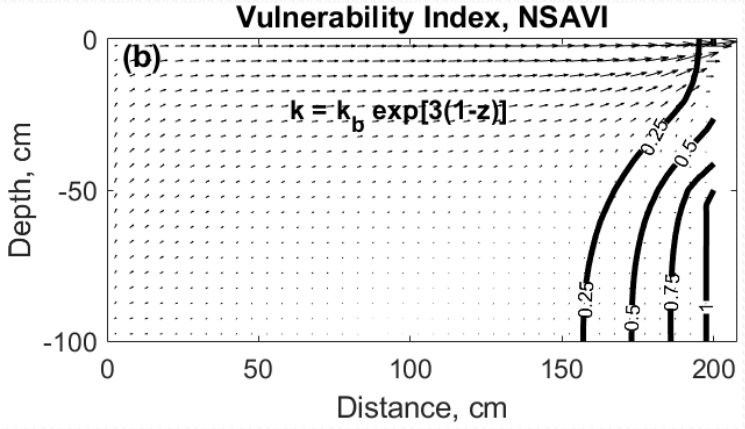

APPLICATION TO AKKAR AQUIFER (LEBANON) (1)

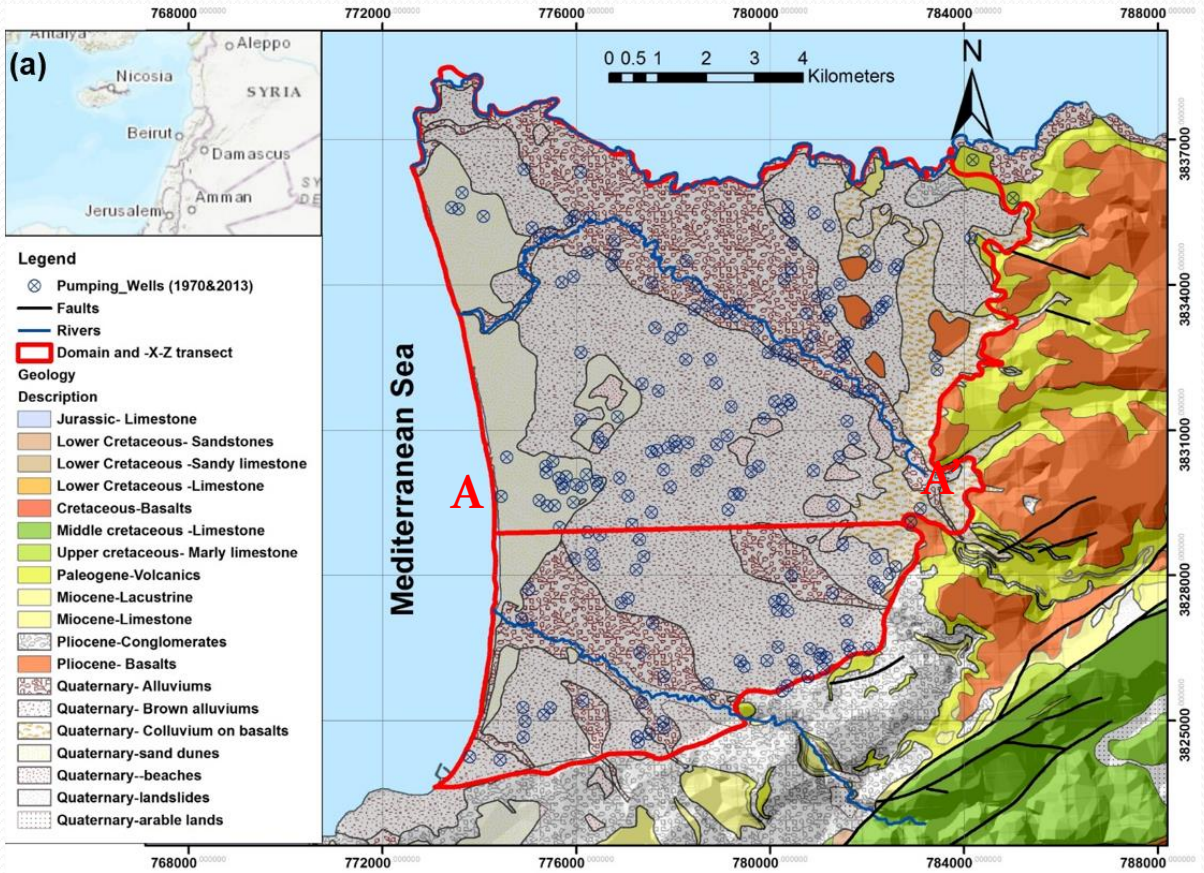

- FAO (1970) and UNDP (2014) studies → 450 mg/l to 655 mg/l in the middle of the plain.
- Increase of water demand for drinking water supply (immigration) and agriculture.
- Examine several short-term management schemes by comparing vulnerability maps.
- Demonstration using the A-A' cross section model.

APPLICATION TO AKKAR AQUIFER (LEBANON) (2)

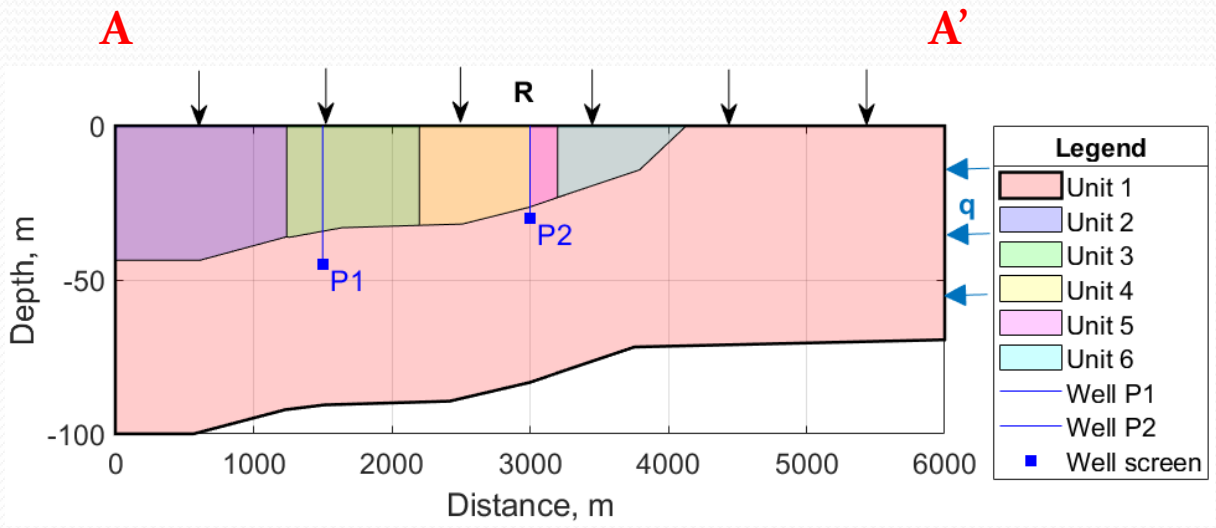

- 6 distinct hydrogeological units (1,2,3 very permeable; 4,5 permeable, 6 impermeable).
- Average recharge R = 100 mm/month (3.8×10^{-7} m/s).
- Lateral recharge q = $6,4 \times 10^{-9}$ m/s.
- Pumping P1 = 579.25 L/h, P2 = 604.25 L/h.
- Strainers at 45 m and 30 m deep, respectively.
- Wells located at 1500 m and 3,000 m from the coast.

APPLICATION TO AKKAR AQUIFER (LEBANON) (3)

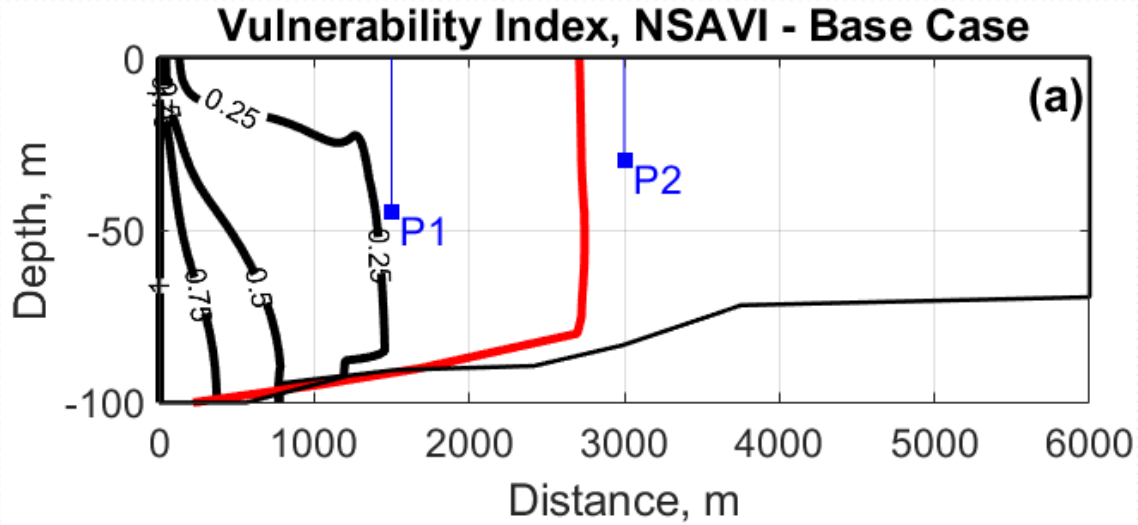

- Vulnerability to seawater intrusion increases with depth.
- The vulnerability gradient increases when approaching the coast.
- The ZVL delineates a risk zone of approximately 2,740 m.

APPLICATION TO AKKAR AQUIFER (LEBANON) (5)

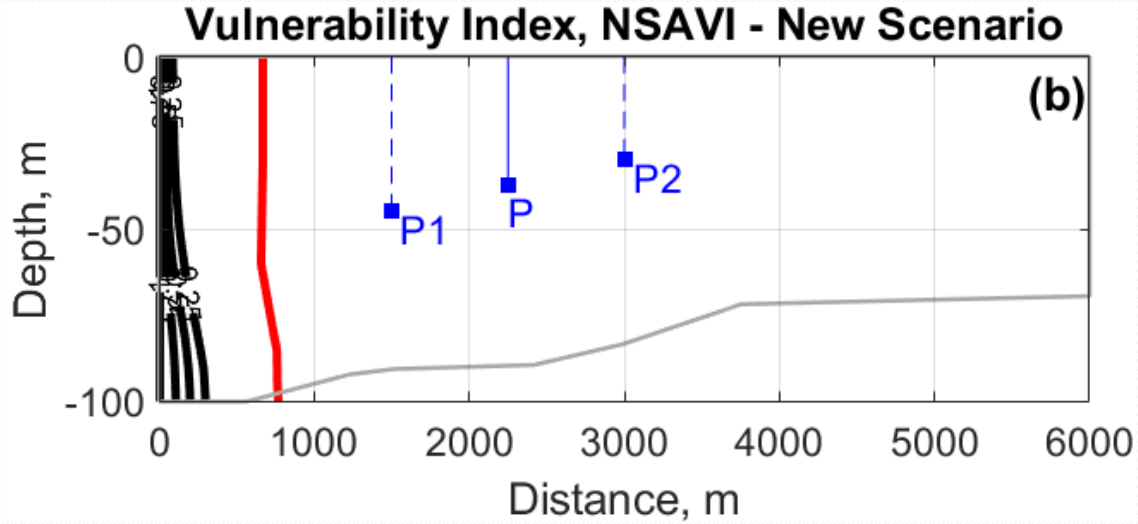

- Testing of several scenarios: (i) moving the wells in XY and Z; (ii) decrease the density of the wells; (iii) reduce the pumping rate.
- Here, a scenario combining these 3 actions with a total flow reduced by 20%.
- The ZVL delineates a risk zone of approximately 760 m → ~ 1/3 of the aquifer space will no longer be under the threat of saline intrusion.
- Demonstration of the usefulness of the concepts introduced for the operational management of coastal aquifers.

CONCLUSION AND RECOMMADATIONS

- New approach reconciling vulnerability mapping in coastal aquifers with advanced practices for modeling variable density processes.

- The NSAVI normalized index is obtained from the **salinity distributions and the mean age of salt water** in a stationary regime.

- In homogeneous aquifers or with heterogeneous stratification, vulnerability increases with depth. **This behavior cannot be reproduced with the previous techniques**.

- The ZVL line delimits the risk areas. This new concept has important implications for optimal resource management and risk assessment.

- The ZVL line is not to be confused with 50% isochlor which is not a robust metric to assess the risk of marine intrusion.

- The theoretical and practical examples provided demonstrate the relevance of this approach to classify, compare and validate the different coastal water resources management scenarios.

CONCLUSION: IMPLICATIONS FOR THE MANAGEMENT OF COASTAL RESOURCES

- The ZVL concept is a new communication tool on seawater intrusion and the impacts of global changes.
- Rapid assessment of the risk associated with the planning of management schemes.
- Prioritize the wells according to the risk of salinization.
- Facilitates the construction of a DSS in an operational setting.
- Parametric or conceptual uncertainty→ stochastic description of the ZVL.
- Acceleration of the simulation-optimization approach → use as a twin model of the coupled transient model.
- Objective function: to move the ZVL line back towards the coast.
- Role in the optimization of the monitoring system and the frequency of measurements.
- The method does not require continuous measurements of the concentration.

REFERENCES

- Kouz T. , H. Cherkaoui Dekkaki, S. Mansour, M. Hassani Zerrouk and T. Mourabit (**2018**): **Application of GALDIT Index to Assess the Intrinsic Vulnerability of Coastal Aquifer to Seawater Intrusion Case of the Ghiss-Nekor Aquifer (North East of Morocco).** Mediterranean Area, Environmental Earth Sciences, https://doi.org/10.1007/978-3-319-69356-9_20

- Sbai, M.A.; Larabi, A. (**2023**): **A Deforming Mixed-Hybrid Finite Element Model for Robust Groundwater Flow Simulation in 3D Unconfined Aquifers with Unstructured Layered Grids.** Water, 15, 1177. https://doi.org/10.3390/w15061177

- Sbai, M.A.; Larabi, A. (**2023**): **Analyzing the Relationship between Doublet Lifetime and Thermal Breakthrough at the Dogger Geothermal Exploitation Site in the Paris Basin using a Coupled Mixed-Hybrid Finite Element Model,** Geothermics 114 102795, https://doi.org/10.1016/j.geothermics.2023.102795

- El Hamidi M.J., Larabi A., and Faouzi M. (**2021**), **Modeling and Mapping of coastal aquifer vulnerability to seawater intrusion using SEAWAT code and GALDIT index technique: the case of the Rmel aquifer – Larache, Morocco**, ICCR 2020, E3S Web of Conferences 298, 0500, https://doi.org/10.1051/e3sconf/202129805002

Credits and Acknowledgements

- OCP (OFFICE CHÉRIFIEN DES PHOSPHATES, MOROCCO)
- MEDAQCLIM EU PROJECT (MEDITERRANEAN FUND)
- MINISTRY OF WATER, ABHL, ONEE…(MOROCCO)

SPECIAL THANKS TO THE CONTRBUTORS TO THESE RESEARCH WORKS: